An electrically-tuneable achromatic laparoscope imaging lens

1. Introduction

Fluorescence image-guided surgery, particularly in the near infrared portion of the optical spectrum is gaining popularity and is increasingly used during a wide range of human surgical interventions. Early applications of this technique used wide-field imaging systems (i.e. using free-space optics) and were limited to open surgery applications. More recently these techniques were extended to keyhole surgery i.e. laparoscopic applications. In particular, molecularly targeted agents are increasingly investigated, particularly for cancer surgery, where their efficacy to ensure that all tumour cells are removed is being evaluated.

The challenge is to develop sensitive imaging systems capable of real-time operation in both the visible (450-650 nm) and the near-infrared (650-900 nm) regions of the optical spectrum. Means of achieving a good sensitivity will be the subject of a separate application note; here we describe an imaging lens that can be used with most types of 10 mm diameter laparoscopes. This lens, as well as being achromatic in the 450-900 nm range has a further property that we consider to be useful for fluorescence image-guided surgery: its focal length is electrically programmable. During fluorescence imaging, signal intensities are inevitably always low and a short working distance is often beneficial. Imaging with a short working distance enhances excitation power density and increases fluorescence emission through the limited diameter laparoscope input pupil. Changing rapidly from a long to a short working distance results in some inevitable defocus and a focus-programmable lens allows the application of appropriate autofocus algorithms. An additional, more practical reason for developing a programmable lens system is that the mechanics associated with a clinical camera become relatively simple. Instead of using a mechanically geared focus rotation system, much simpler ‘focus up’ and ‘focus down’ switches can be implemented. This latter approach is much more straightforward, particularly in non-commercial, research applications.

There is in principle nothing too exceptional in developing an achromatic system; most optical design software tools will readily optimise a design. The trouble is that the resulting lenses may well be unobtainable economically, at least in low quantities. In our design, we utilise ‘off-the-shelf’ components throughout, components that are readily available from suppliers that are active in the UK.

We also describe here an efficient electronic driver circuit used to program the focal length of the variable element. Although there are numerous ways of achieving this, we describe here an electrically efficient design which can be constructed in a way that is small enough to fit inside a camera assembly.

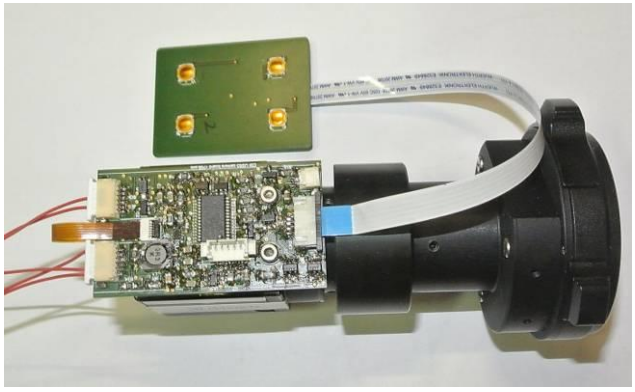

Figure 1: The completed programmable imaging lens, its drive circuit and control switches, fitted around a small camera.

1. Laparoscope optical characteristics

The modern rigid laparoscope was first developed by HH Hopkins in the late 1950s-early 1960s. His use of thick ‘rod’ lens endoscopes made possible modern keyhole surgery. His elegant solution to the problem of minimising glass-air surfaces in a multi-lens telescope was to use glass rods to fill the air-spaces between the objective and the eyepiece lens assemblies (and other relay lenses, now restricted in number (see https://en.wikipedia.org/wiki/Harold_Hopkins_(physicist) for further details)). Of course it was HH Hopkins who also laid the foundation of Fourier optics and developed the concept of the Modulation Transfer Function, indeed pretty well all the mathematics exploited in the ZEMAX (http://www.zemax.com/) optical design package that we used to develop our imaging lens. Rather than

use a lot of words to describe the principle of this wonderful optical instrument, the reader may find it more instructive to view an X-ray image of a typical laparoscope, as shown in Figure 2.

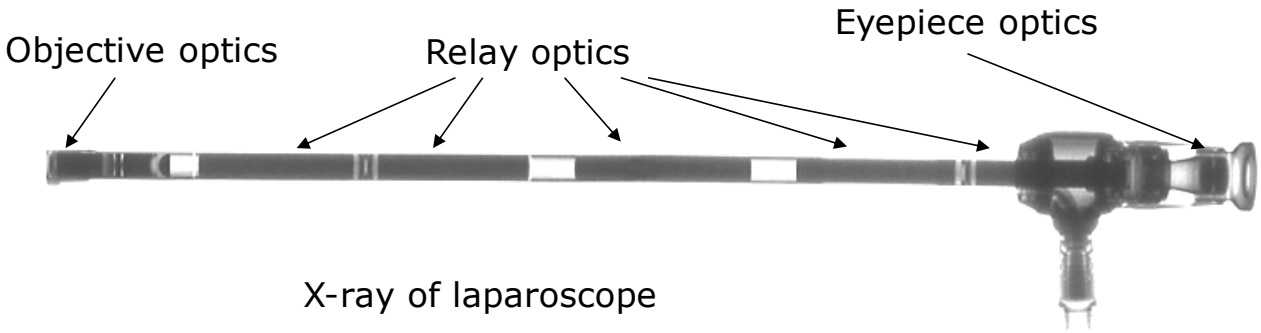

Figure 2. X-ray image of a typical rigid laparoscope. Thanks to Anthony Kavanagh who acquired this image which shows clearly the relay solid rod lenses

Of course the prescription of the individual optical components is usually a rather closely guarded commercial secret; although some information can be gleaned from various patents, the amount of work required to translate the various optical parameters into numbers that ZEMAX works with is not trivial. Suffice it to say that the output of the laparoscope eyepiece is near-collimated ray bundles from every point in the object field, as shown in Figure 3. Is the laparoscope achromatic over our working range? Probably not. It is however, much easier to determine how chromatic it is, particularly in the NIR when we have at our disposal a reasonably achromatic imaging lens of known prescription to work with; using it, we can determine the laparoscope performance and perhaps in the future design a superior imaging lens.

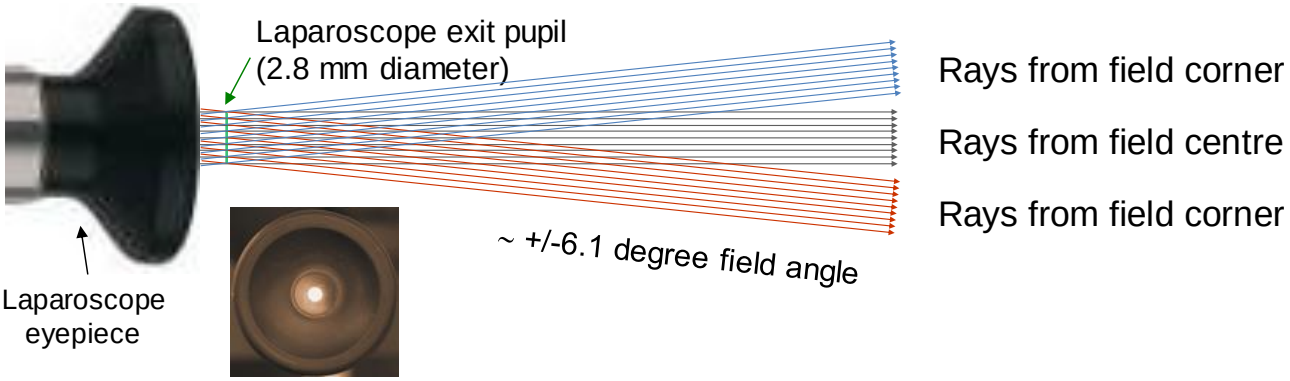

Figure 3. The output rays from a typical 10 mm diameter rigid laparoscope. The laparoscope eyepiece is matched for good performance with the human eye and the output field angle is typically ~±7 deg. at full field. However, the illumination power density falls off at the field edges, resulting in apparent vignetting. The use of a more restricted ~±6 deg. output angle provides a relatively 'flat' illuminated image. The ray bundle diameter is typically of the order of 2.8 mm and the output pupil is arranged to be outside the eyepiece, a few millimetres in front of the output window.

The job of the imaging lens is to bring these bundles into focus in an image plane, where a camera sensor would normally be placed. The focal length of this imaging lens depends on the sensor dimensions: the larger the sensor, the longer the focal length. In practice, and particularly for fluorescence imaging, a small sensor is generally preferable because the camera assembly should be as short as possible, suggesting the use of a short focal length sensor. We settled on an imaging lens with a nominal focal length 28 mm nominal. This allowed us to use a 6 mm diagonal sensor (1/3" format.)

It is worth pointing out that that the spatial resolution is restricted by the diameter of the ray bundle which has a typical diameter of 2.8 mm, as mentioned before. The radius of the resulting Airy disc will thus

depend on the lens focal length (https://en.wikipedia.org/wiki/Airy_disk) and on the wavelength. Figure 5 shows how the Airy disc radius varies with imaging lens focal length and how it varies as wavelength is changed for our chosen 28 mm focal length. This pupil-defined limitation informs us on how good our lens needs to be: over-specification in any field of engineering is usually pointless. This limitation shows us that in the NIR, at 900 nm, our Airy disc will have a diameter of 22 μm – an inevitable limitation due to the behaviour of light waves.

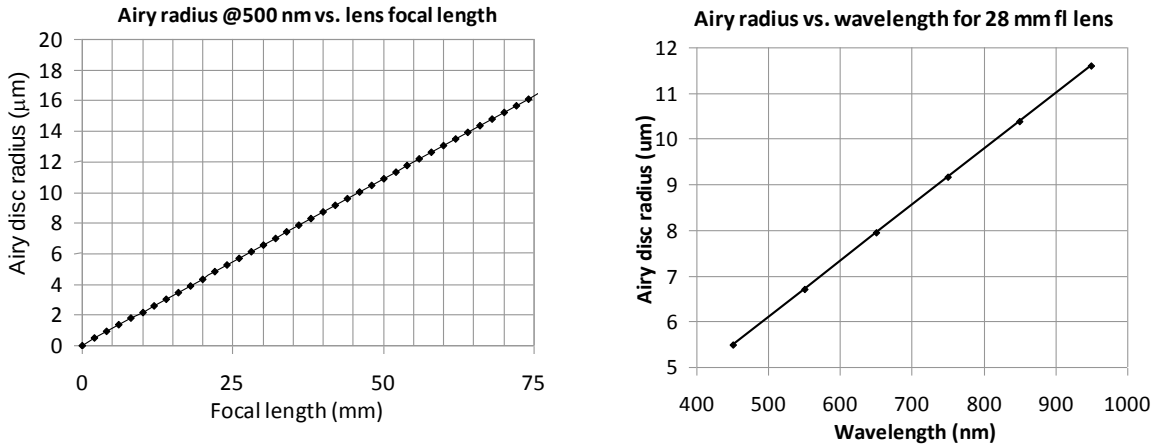

Figure 5. Left: Variation of Airy disc radius with imaging lens focal length with a 2.8 mm diameter pupil when imaging a 500 nm wavelength. Our chosen 28 mm focal length results in a ~6 μm Airy disc radius when using green light. Right: Variation of Airy disc radius as a function of wavelength for our chosen 28 mm focal length lens.

It is also worth pointing out that laparoscopes designed specifically to work in the NIR also feature increased transmission, presumably due to improved coatings on the internal optical elements. Such a comparison, using Storz laparoscope type 26003 AA and laparoscope type 26003 AGA, the latter designed for NIR work, is shown in Figure 6.

Unfortunately, we did not have access to many different types of laparoscopes, and the data presented in Figure 6 should be taken only as a guide.

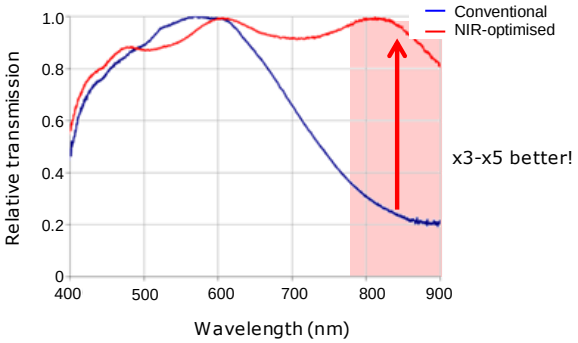

Figure 6. Improved transmission of NIR-optimised laparoscope. Please refer to text for laparoscope model numbers.

2. Imaging lens design

The lens design was performed with the aid of the ZEMAX modelling package. A number of configurations were tried using lenses available from Edmund Optics (www.edmundoptics.com), Thorlabs (www.thorlabs.com) and Comar Instruments (www.comaroptics.com) as these were our most commonly used and reliable suppliers of optical components. Doubtless there are others that we could have investigated. There were two principle issues that need to be optimised: achromatic performance and field flatness. In general, it is always better to place the programmable lens as the first element, since then only focusing is performed rather than both focusing and magnification changes when the programmable lens focal length is varied. However, we could not achieve the level of field focus flatness and achromatic performance by using the programmable lens as the first element in the imaging lens optical train. The eventual design, obtained after trying out numerous approaches using many optical components from numerous manufacturers is shown in Figure 7. Patience is indeed a virtue when performing optical design!

When using combined fluorescence and white light imaging, it is relatively straightforward, though often expensive (!) to use narrow band notch filters, tuned to the excitation wavelength(s), placed directly after the laparoscope. Multilayer coated filters can usually accept a ±6 degree ray cone without too much loss of performance (see e.g. https://www.semrock.com/filter-spectra-at-non-normal-angles-of-incidence.aspx or https://www.semrock.com/mylight-tutorial.aspx for ways to check the performance of notch filters with a specific cone angle.) Furthermore, by placing the filters in the optical infinity space, spherical aberrations are minimised. It is for this reason that we placed our first lens at some distance from the laparoscope exit pupil; there is enough room to place a number of thin filters in this space, even if these are 2.5- 3 mm thick. In practice we use custom-made filters of 1.1 mm thickness.

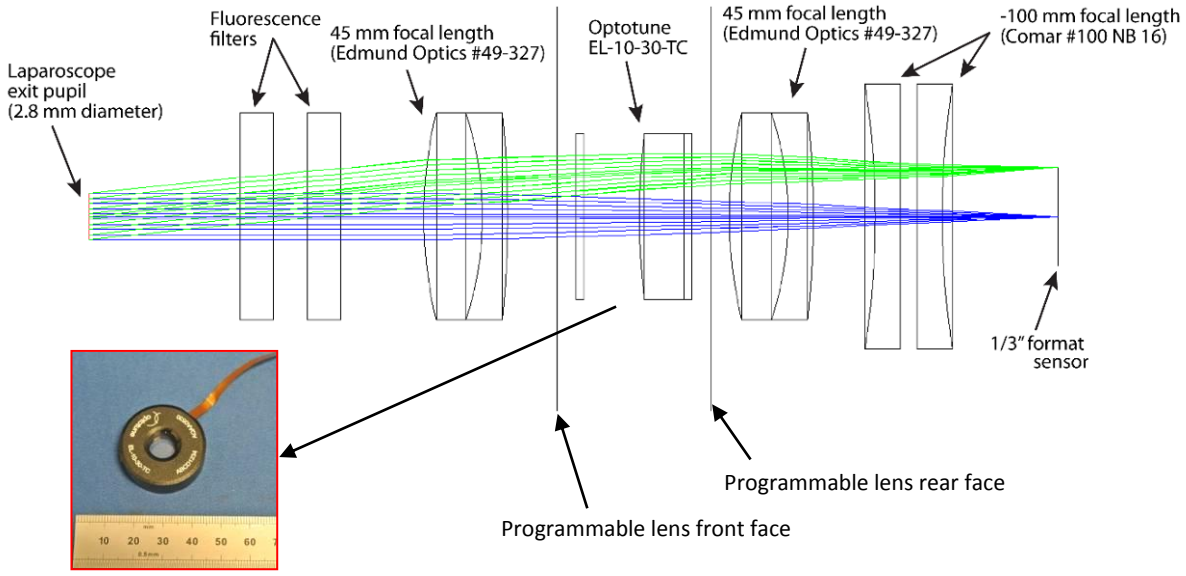

Figure 7. Optical ray tracing for our 28 mm focal length configuration (6 mm diagonal sensor format.) The minimum (0 degrees) and maximum (6.1 degrees) field angles are shown in blue and green respectively. The programmable lens (lower image) optical performance was determined from the manufacturer material data. Similarly, the prescription of the conventional lenses was obtained from their respective suppliers.

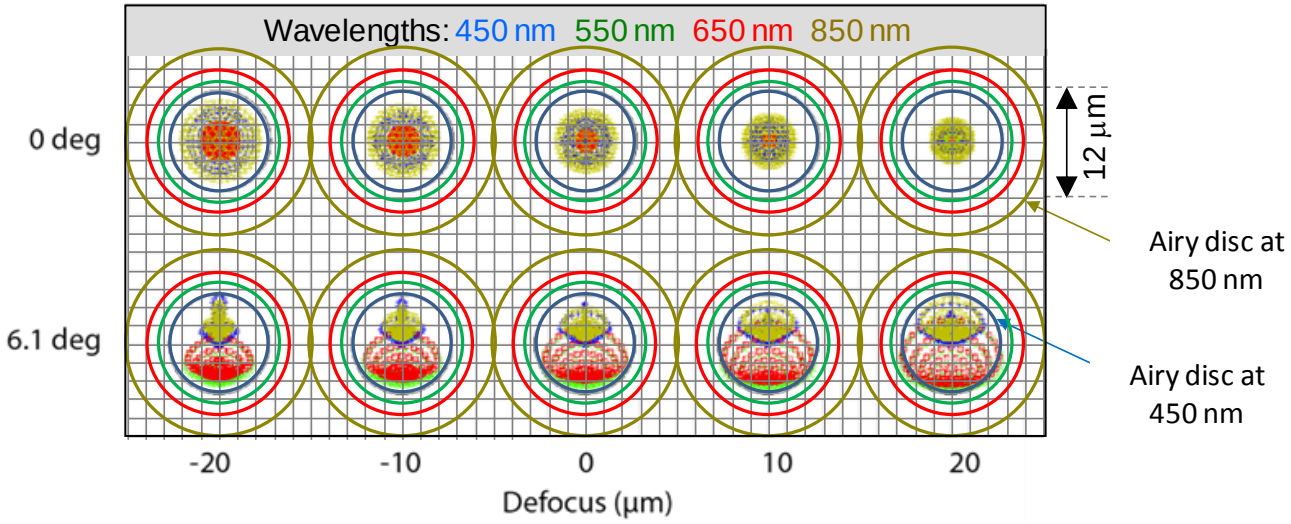

Figure 8. Spot diagrams in the image plane, through the optimal focus, showing all the system wavelengths to be within the smallest Airy disc appropriate for a wavelength of 450 nm. Resolution-limiting Airy discs at wavelengths up to 850 nm are also shown, according to the colour code shown at the top of the diagram. These data, and imaging measurements, not shown here, confirm that lens is indeed achromatic well into the NIR.

It is worth noting that we designed this arrangement such that the programmable lens operates near the bottom part of its current range, i.e. with the lowest operating current. The reader is strongly encouraged to visit the Optotune web site (www.optotune.com/) and become familiar with the details of this novel lens, particularly if duplication of this system is envisaged.

The reward for all the patience was a relatively simple design with very good performance indeed, as exemplified in Figure 8. It is stressed again that our aim was to use off-the-shelf components; since aplanats are rarely available, we were forced to use an approximation developed with a pair of negative lenses. We do hope that suppliers of optical components will consider in the future supplying a range of aplanats, essential for obtaining a good flatness of field. Of course, Figure 8 depicts theoretical performance and does not take into account inevitable centration issues and lens-lens distances. Such limitations degrade the practical performance somewhat, but not too much, as will be shown later. We operate the Optotune EL-10-30-TC lens over a 170 to 85 mm focal length range, corresponding to 25.3 to 29.2 mm focal length range of the composite lens. This range allows close work with most laparoscopes.

4. Lens mechanics

The housings for the lenses shown in Figure 7 were designed with the aid of the Solidworks mechanical modelling package (www.solidworks.co.uk) Readers who may wish to modify this can use a trial version obtainable from www.cadtek.com/solidworks-trial. Our design files can be made available on request. Viewers are also available (e.g. www.solidworks.co.uk/sw/products/free_2d_tools.htm.)

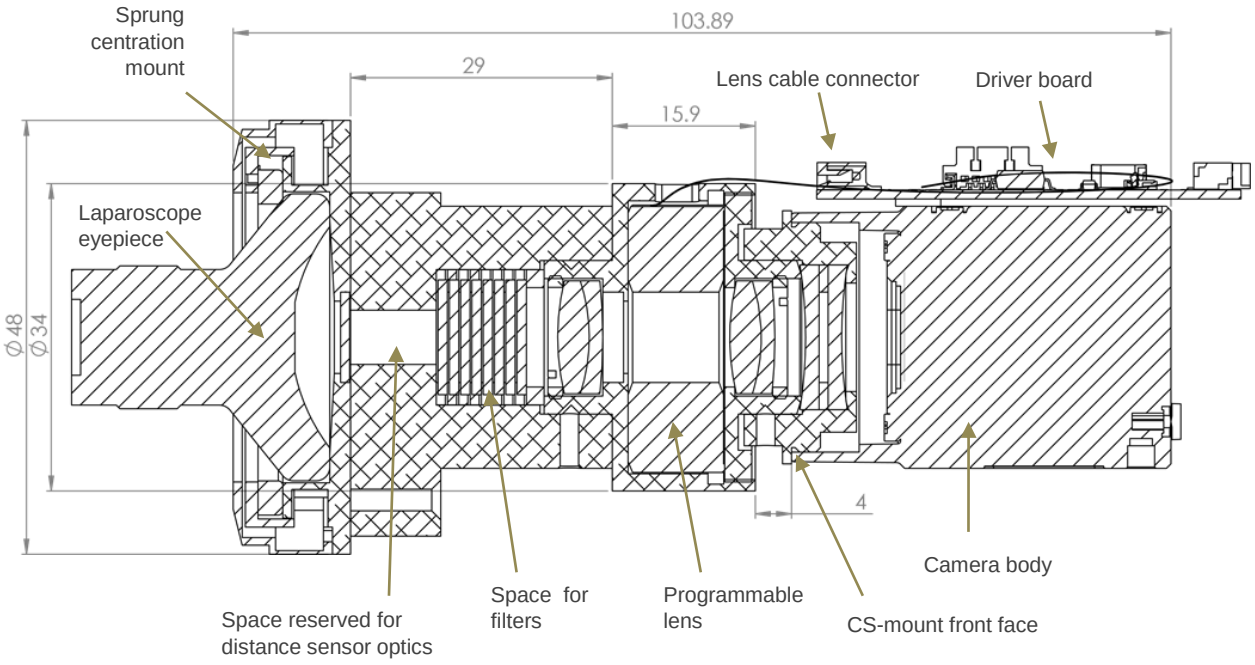

Figure 9. Solidworks drawing of the lens housing, shown attached to the laparoscope and to a Point Grey Blackfly camera. There is space for up to eight fluorescence excitation rejection notch filters. Space is also reserved for distance sensor optics before the fluorescence excitation filters. Scale is 1.25:1 when printed on A4 paper.

The details of the design are depicted in Figures 9 and 10. All components were machined from aluminium and black-anodised. There were two principle challenges in the mechanical development. The first concerns the mounting of the programmable lens. Here the issue is to arrange for the lens electrical connections (flexible printed connections) to be available outside the housing through a slot. Unfortunately the programmable lens has to be handled differently from other optical components. A related feature is that we wanted the filters to be readily accessible and this was achieved with a dovetail coupling. The second challenge was to develop a means of coupling the lens assembly to the laparoscope eyepiece. Here we freely admit to cheating, or, since we want to sound professional, to apply reverse engineering. We used a low cost commercial laparoscope camera lens assembly (Lenoptec LEOA28, www.lenoptec.com) and copied its intricate spring-loaded coupling mechanism. Why modify a good design?!

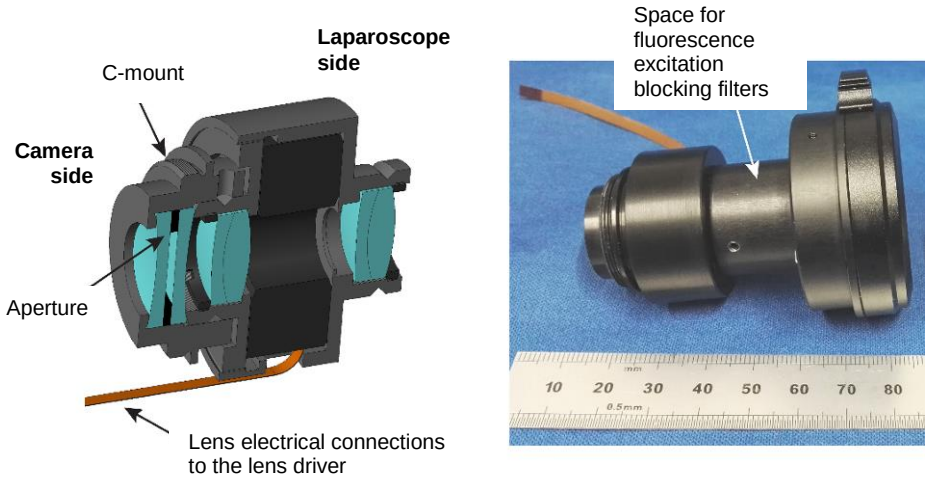

Figure 10. Left: CAD model section view of the custom housing that holds the optical components. A field-defining aperture restricts the possibility of stray reflected light from reaching the camera sensor. Right: image of the competed lens, also including a clamp to fit on the vast majority of laparoscopes.

5. Lens driver

The programmable lens shape, i.e. its focal length is defined by passing current through a solenoid. This current should not exceed 300 mA and, since the solenoid resistance is of the order of 15 Ω, this defines the maximum voltage applied to the lens as 5 V. The solenoid inductance is ~200 μH. The DC characteristics thus suggest that the lens would dissipate up to 1.5 W when it is operated at its shortest focal length. This power level was considered to be excessive, particularly as many modern small CCD/CMOS cameras consume not much more than 2 W. It is always useful to minimise heat generated as much as possible, in what is after all a hand-held instrument. We have limited the operating current to 150 mA, or <350 mW in our optical design. Similarly, the use of an analogue current regulator was to be avoided since this wastes power unnecessarily. We therefore opted for an approach based on a switching regulator. Here we make use of the fact that that the high inductance (and long mechanical time constant) of the lens solenoid allows us to drive it with a variable mark-space, 0-to-5 V amplitude square wave at a frequency of 31.25 kHz. In effect, the solenoid inductance serves as the switcher power transfer coil. Subsequent circuits may be more easily understood by referring to the block diagram of our driver/controller, shown in Figure 11. All the control functions are performed in a PIC (Microchip) microcontroller. The coil current is sensed by developing a low voltage across a sense resistor and high frequency components are filtered with a ~195 Hz low pass filter (τ = 820 μs). This filter also serves as a simple anti-aliasing filter (>40 dB down at 31.25 kHz) for subsequent analogue-to-digital conversion, performed to 10 bit resolution in the PIC ADC. Two conversions are performed within a few tens of microseconds after one another and averaged. This process is repeated every 410 μs and provides a feedback signal to a digital, but otherwise conventional proportional controller. At this point a few deviations from convention start. A track-and-hold routine in the feedback loop is included to allow focus

changes only after a camera synchronisation pulse, which occurs in between camera frames, typically present every 20 or 40 ms (50 Hz or 25 Hz frame rate.) Such a synchronisation aids the operation of any potential future autofocus routines. We then restrict the data drive to a pulse-width modulator (PWM) internal to the PIC. This pulse-width modulator operates at a 10 bit resolution, a resolution fine enough to allow several levels to occur across a barely perceptible focus change of the lens assembly, but prevention of rollover is essential, allowing only levels 0-1023 to be fed to the pulse width generator block. The digitised lens current is also fed to a software comparator which senses a potential over-current condition and reports this to the host software system.

Now comes the 'awkward' part of the operating procedure; we say awkward because part of it could, but does not, contain proprietary information from Optotune. We are bound by a non-disclosure agreement with Optotune concerning lens characteristics present in a memory chip within the lens. The issue here is that the focal length of the programmable lens varies with temperature. The lens temperature is measured within the lens, with a digital thermometer chip, which also contains proprietary correction information. The intra-lens electronics communicate these data through an independent I^2C link. Details of the I^2C communication protocol can be found at www.i2c-bus.org/i2c-bus/. Although two busses are shown in Figure 11, in reality both the temperature and the lens calibration data come down a single I^2C bus. We also read the actual temperature and send this to a host controller, through a separate I^2C bus…just to make it confusing! This second I^2C bus is bi-directional and allows the host to set the working lens focal length. A set-point limiter is also included, limiting the maximum set point current to ~150 mA. Finally, the bus to the host is also used to relay button presses from local control push-button switches. The functions of these switches is determined in the host controller, typically arranged as manual up-down focus control or autofocus up-down controls; they can also be used to control the sensitivity of the local camera. These functions are not discussed in detail here.

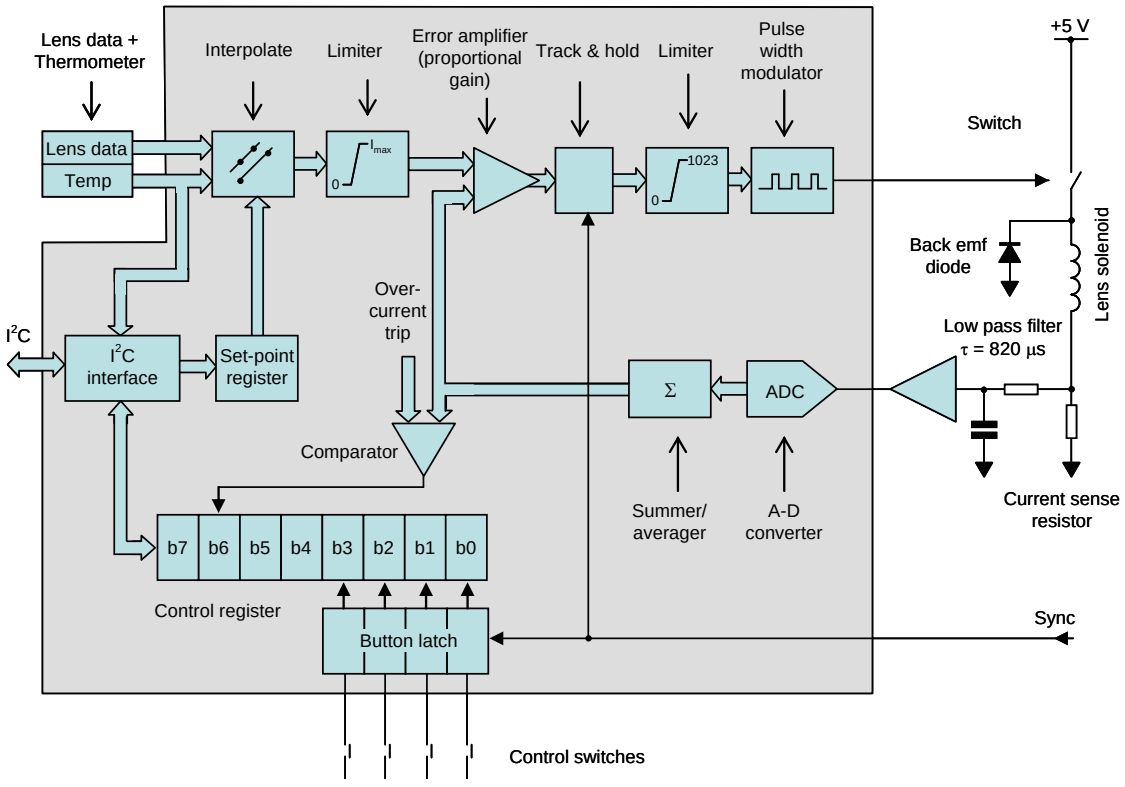

Figure 11. Block diagram of the lens control electronics. Please see text for details.

A partial, though detailed circuit diagram of the lens driver is shown in Figure 12. The lens houses a NXP SE97B temperature sensor which provides temperature data on a 3.3V level I^2C bus. All the electronics are powered by 5V. However, since most cameras require a +12V supply, we use this voltage to provide primary power and provide a low power switching buck converter (U4) to convert this to +5 V.

This lens pulse-width-modulated drive is provided by a PMOS switch (Q2) and any lens-inductance-generated back-e.m.f. is absorbed by a Schottky diode (D1). The PMOS switch is driven by a gate driver (U1) with the PWM signal itself provided by the PIC (U3). The PIC uses external 5V level I^2C information (on pins 22, 23) and/or inputs form push-button switches (SW1-4) to determine the PWM duty cycle, along with 3.3V level I^2C temperature data and with lens solenoid current. The control switches SW1-4 are processed with a pair of de-bounce chips (U6, U7); these could be eliminated and replaced by the PIC software, but their additional cost is well-warranted here and eliminates added software development. Similarly, Q1a, Q1b, R8 and R9 could be eliminated if cost is an issue, but we thought it safer to use a well-proven method[1] of I^2C voltage level conversion. The gate driver (Q1) also includes a linear 5V to 3.3V regulator and this was exploited to power the lens temperature sensor.

Lens current, typically less than 150 mA, is sensed by R3; PWM variations are smoothed by a low pass filter (R4 and C2) and scaled to ~4.1 V by the operational amplifier U2. One of the PIC's A-D converters is used to sense this current, while the A-D reference voltage (4.096V) is provided by a 2-terminal reference, U5.

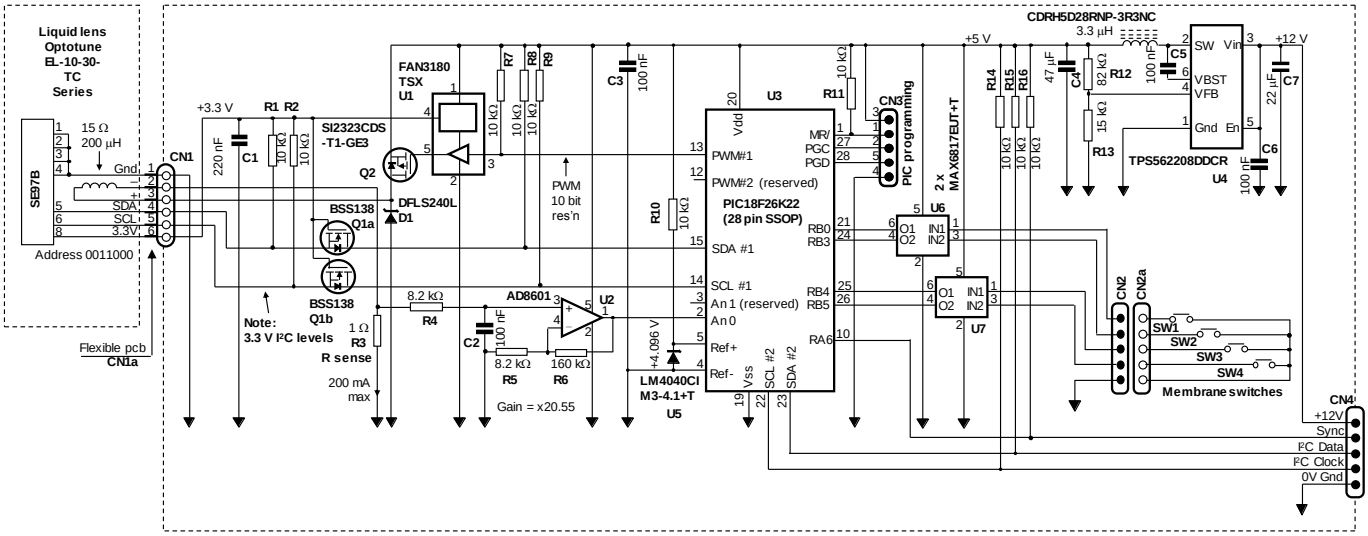

Figure 12. Basic electronic circuit of the lens driver. Please refer to text for details.

The PIC chosen is capable of PWM driving two programmable lenses (e.g. as may be used in the future in a zoom arrangement) and pins 12 and 3 are served for such expansion if required. In the simplest arrangement, two of the input switches are used to increase/decrease the lens dioptre value while the other pair may be used for other system control functions (e.g. sensitivity or imaging modes). We note that the specifications of the lens are provided by Optotune in dioptres (equal to the reciprocal of the focal length measured in metres (i.e. in units of m^{-1})). The required functions are determined by the PIC software, loaded in on the programming connector CN3.

In our application, we also provide a 'sync' input to the PIC (pin 10) which can be used to ensure that lens movement is made possible only in between imaging frames.

Figure 12 depicts a perfectly workable arrangement that could be constructed to work stand-alone. In our specific application, however, we use the circuit shown in Figure 13.

Here we provide additional connectors and electronics to add functionality. The first is the addition of contacts for a tilt switch, used elsewhere in the host controller and not described here. When performing fluorescence imaging, often large (several watt) excitation powers are sometimes necessary. In the NIR in particular, the excitation light is invisible, or barely visible. We fit a tilt switch which acts as an excitation interlock, switching off the excitation source at specific orientation angles of the camera. The excitation light is thus prevented from exiting the laparoscope tip, potentially endangering personnel. This feature is

[1] NXP Application note AN10441 Level shifting techniques in I2C-bus design, Rev. 01 — 18 June 2007

mostly useful when the board is used with a camera intended for open surgery application, i.e. when the camera is normally operated above the object.

The second addition is U5 and Q3. These are used to drive a light source used in conjunction with a distance sensing arrangement. This arrangement is not described here in detail, but nevertheless we have to allude to it since the more observant reader will examine the printed circuit board layouts and discover components not present in the circuit shown in Figure 12.

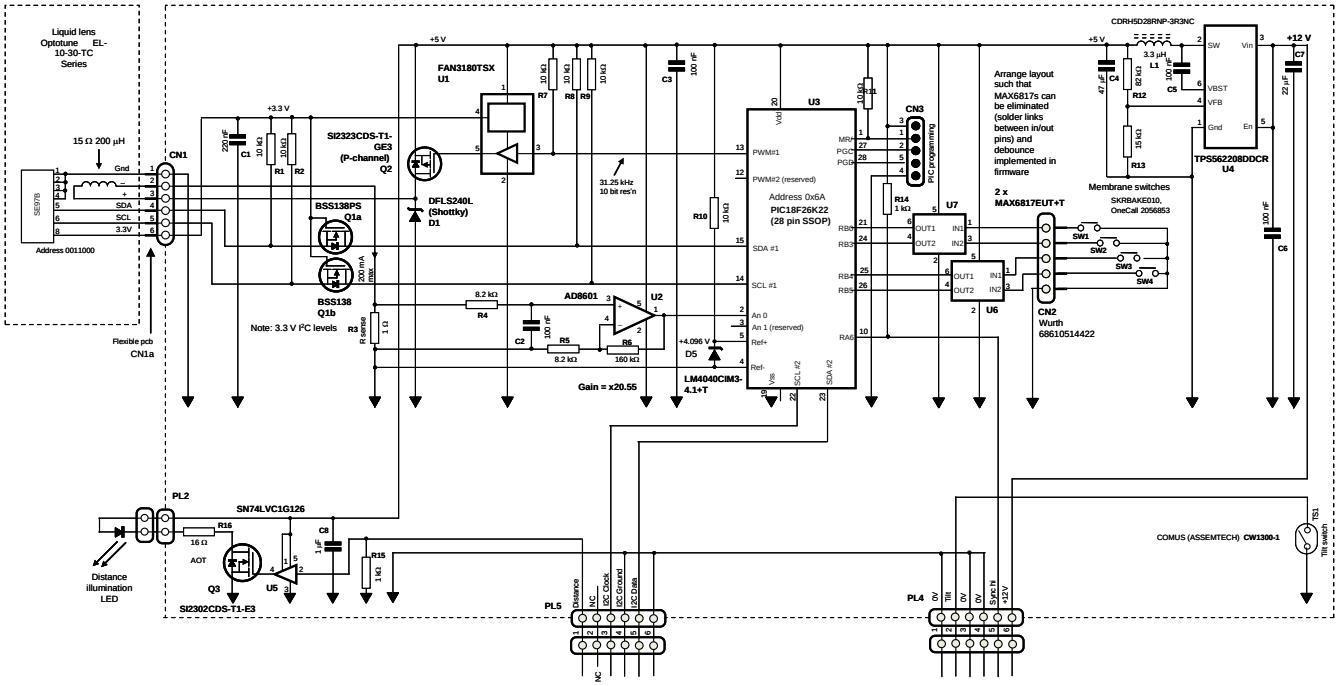

Figure 13. Complete circuit diagram of the camera add-on board. Please refer to text for details.

The electronics are constructed on a 1 mm thick double-sided printed circuit, 47 x 27 mm, small enough to fit close to the body of our camera. The component packing is rather dense and could be relaxed if smaller surface-mount components were used. However, as most of our team assembling printed circuit boards require magnifiers of increasing power (yes, we are all getting ever so slightly old!) we generally restrict ourselves to using 0805 size passive components.

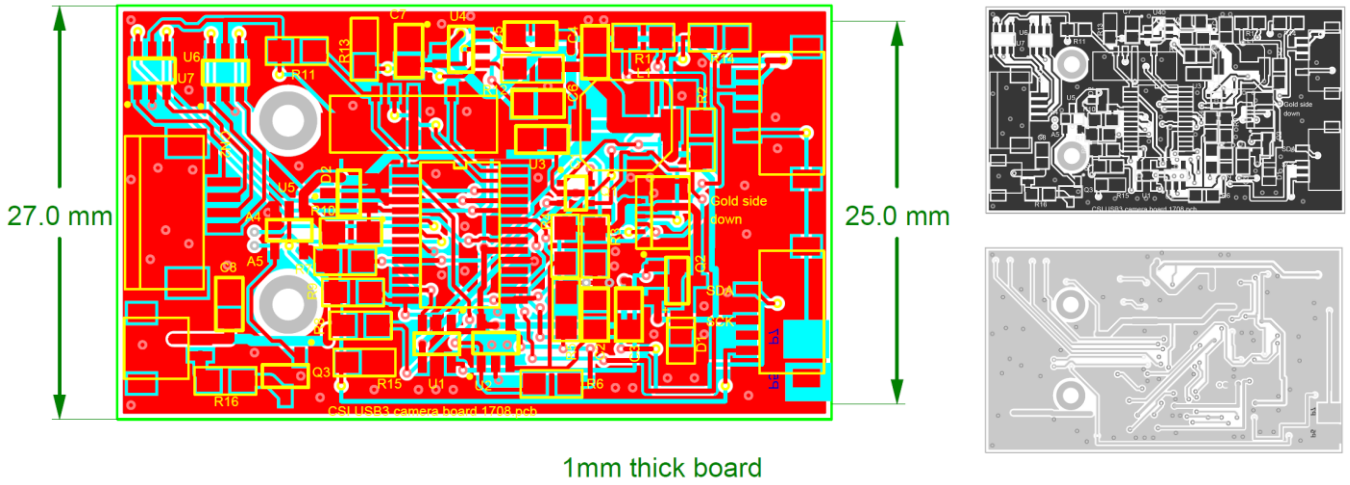

Figure 14. Printed circuit board layouts of the lens driver board. The complete design is shown on the left (2x magnification, when printed on A4 paper) with the top (top right hand side of the figure) and bottom (bottom right had side of the figure) layers shown in real size on right.

We say once again, the component packing *is* dense and if this is your first surface mount printed circuit assembly project, then don't attempt it!

The printed circuit layout was developed using EasyPC software (www.numberone.com). Design files can be supplied on request but we are not able to translate these into other circuit design software tools.

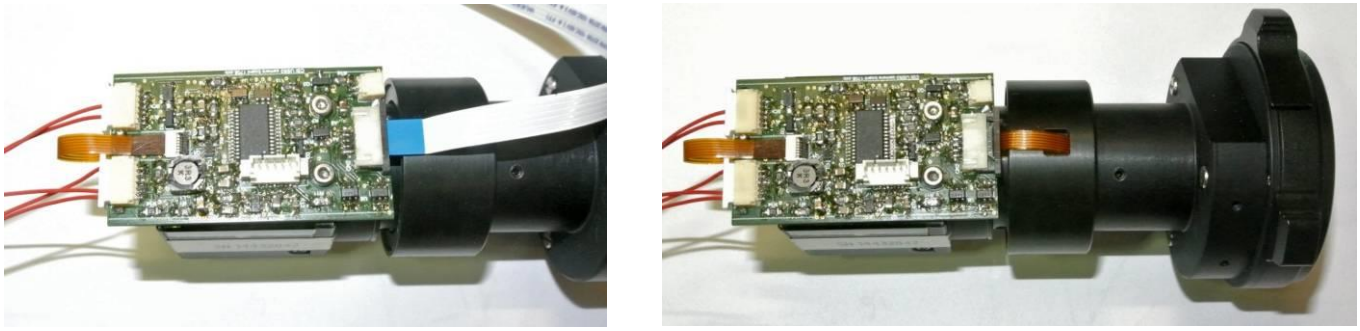

Figure 15. The printed circuit board attached to the camera and lens. Left: push-button switch cable plugged in, obscuring the lens flexible cable. Right: The lens cable is apparent, passing under the board and plugged into a socket on the left half of the board. The programming socket is just under the PIC, bottom centre of the board.

For completeness, a second board, as depicted in Figure 1 as part of the complete system, is shown in Figure 16. This board only holds the control switches and a connector.

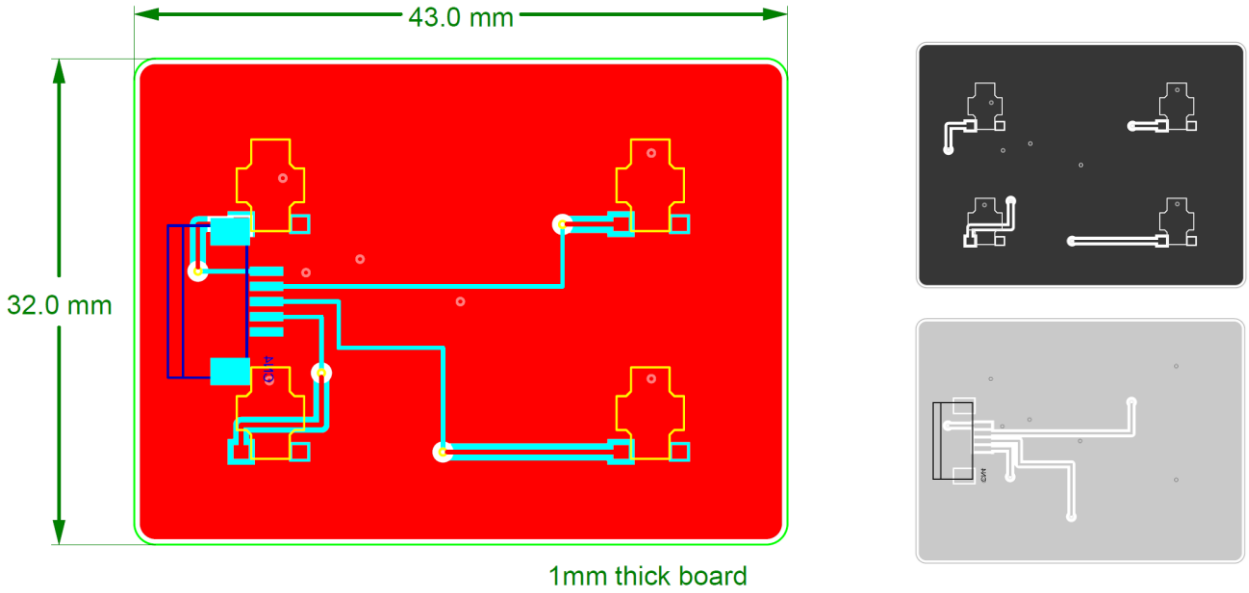

Figure 16. The printed circuit board onto which are mounted the control switches. Compared to Figure 14, this board I simplicity itself! Image scaling and positions of the layer images are as in Figure 14.

None of the electronic component specifications are particularly special. A component list is provided in Table 1. Although several suppliers are listed in the table, we used these as a matter of internal convenience. The total cost of the electronic components is low, below £30. This makes up for the high cost of the programmable lens itself and that of other optical components, shown in Table 2.

The double-sided printed circuit boards were made as custom parts by Beta Layout, a company (www.beta-layout.com/) who provide a convenient service from EasyPC files supplied to them. It is noted that the lens driver printed circuit board layout, specifically the location of the mounting holes, was

designed to fit the Blackfly range of camera obtainable from www.ptgrey.com/, and arranged to be attached onto tapped mounting holes present on the camera. Similarly, the position of the lens flexible cable is determined by the placing of the Optotune lens within our assembly.

Table 1: Lens driver component listing

ID	Item	Description	Model #	Supplier	Part number	Price
--	Printed circuit board Double-sided	Filename: CSI USB3 camera board 1650.pcb	Part of switch board	Beta Layout	---	10.17
U1	MOSFET driver and regulator	Gate Drivers Single 2 A Low-Side Driver w/ 3.3V LDO SOT-23-5	FAN3180TSX	Mouser	512-FAN3180TSX	0.779
U2	Lens current sensor	Precision Amplifiers RRIO Single, low offset	AD8601	Mouser	584-AD8601ARTZ-R7	1.09
U3	Processor	8 Bit Microcontroller, Flash, PIC18FxxKxx, 64 MHz, 64 KB, 3.8 KB, 28 Pins, SSOP	PIC18F26K22T-I/SS	OneCall	2429022	1.85
U4	Switching regulator	4.5V to 17V Input, 2A Output, Synchronous Step-Down Converter 6-SOT -40 to 85	TPS562208DDCR	Mouser	595-TPS562208DDCR	0.734
U5	Switch debouncer	DUAL, +/-25V, 6SOT23	MAX6817EUT+T	OneCall	2519143RL	3.34
U6	Switch debouncer	DUAL, +/-25V, 6SOT23	MAX6817EUT+T	OneCall	2519143RL	3.34
U7	Buffer/gate driver	Buffer, Non-Inverting, 3-State, 1.65V to 5.5V, SC-70-5	SN74LVC1G126DCKR	OneCall	1621010	0.127
Q1	Dual Mosfet Level shifter	Dual MOSFET, Dual N Channel, 320 mA, 60 V, 0.9 ohm, 10 V, 1.2 V	BSS138PS	OneCall	1972664	0.087
Q2	PMOS lens switch driver	MOSFET 20V 6A P-CH MOSFET - 20 V - 6 A 32 mOhms	SI2323CDS-T1-GE3	Mouser	781-SI2323CDS-T1-GE3	0.535
Q3	NMOS distance sensor driver	MOSFET 20V 2.9A 0.86W 57 mohm	SI2302CDS-T1-E3	Mouser	781-SI2302CDS-E3	0.321
R1	3.3 V I²C pullup resistor	10 kΩ 1% 0805 100 mW	MC 0.1W 0805 1% 10K	OneCall	9332391	0.02
R2	3.3 V I²C pullup resistor	10 kΩ 1% 0805 100 mW	MC 0.1W 0805 1% 10K	OneCall	9332391	0.02
R3	Lens current sense resistor	1 Ω 0805, 250 mW, ± 1%, LRCS Series	LRCS0805-1RFT5	OneCall	1506147	0.087
R4	Lens current low pass filter resistor	8.2 kΩ 1% 0805 100 mW	MC 0.1W 0805 1% 8K2	OneCall	9333584	0.002
R5	Lens current gain set resistor	8.2 kΩ 1% 0805 100 mW	MC 0.1W 0805 1% 8K2	OneCall	9333584	0.002
R6	Lens current feedback resistor	160 kΩ 1% 0805 100 mW	MC 0.1W 0805 1% 160K	OneCall	9332685	0.002
R7	PWM source pull-up resistor	10 kΩ 1% 0805 100 mW	MC 0.1W 0805 1% 10K	OneCall	9332391	0.002
R8	5 V I²C pullup resistor	10 kΩ 1% 0805 100 mW	MC 0.1W 0805 1% 10K	OneCall	9332391	0.002
R9	5 V I²C pullup resistor	10 kΩ 1% 0805 100 mW	MC 0.1W 0805 1% 10K	OneCall	9332391	0.002
R10	Voltage reference series resistor	10 kΩ 1% 0805 100 mW	MC 0.1W 0805 1% 10K	OneCall	9332391	0.002
R11	PIC master reset pullup resistor	10 kΩ 1% 0805 100 mW	MC 0.1W 0805 1% 10K	OneCall	9332391	0.002
R12	Switcher voltage set feedback resistor	82 kΩ 1% 0805 100 mW	MC 0.1W 0805 1% 82K	OneCall	9333592	0.002
R13	Switcher voltage set gain resistor	15 kΩ 1% 0805 100 mW	MC 0.1W 0805 1% 15K	OneCall	9332618	0.002
R14	Sync pulse pullup resistor	1 kΩ 1% 0805 100 mW	MC 0.1W 0805 1% 1K	OneCall	9332383	0.002
R15	Distance set input pulldown resistor	1 kΩ 1% 0805 100 mW	MC 0.1W 0805 1% 1K	OneCall	9332383	0.002
R16	Distance sense output current limit	16 Ω 500 mW, ± 1%, ERJP06 Series	ERJP06F16R0V	OneCall	1894161	0.102
C1	3.3 V I2C decoupling capacitor	220 nF, X7R, 220NF, 0805, 50V	08055C224KAZ2A	OneCall	2332797	0.204
C2	Lens current low pass filter capacitor	100 nF 0805, 50V	08055C104JAT2A	OneCall	1740673	0.068
C3	5V decoupling capacitor	100 nF 0805, 50V	08055C104JAT2A	OneCall	1740673	0.068
C4	5V decoupling capacitor	47 µF MLCC - SMD/SMT 0805 47uF 6.3V	GRM21BR60J476ME15L	Mouser	81-GRM21BR60J476ME5L	0.314
C5	Switcher boost capacitor	100 nF 0805, 50V	08055C104JAT2A	OneCall	1740673	0.068
C6	12V DC input decoupling capacitor	100 nF 0805, 50V	08055C104JAT2A	OneCall	1740673	0.068
C7	12V DC input decoupling capacitor	22 µF Ceramic MLCC - SMD/SMT 0805 16 volts X5R 20%	GRM21BR61C226ME44L	Mouser	81-GRM21BR61C226ME4L	0.285
C8	Distance sensor decoupling capacitor	1 µF, 25V, 0805, MLCC, X7R,	GRM219R71E105KA88D	OneCall	1845770	0.156
CN1	Lens drive and feedback header	Receptacle to lens FFC / FPC 503480 Series	503480-0600	OneCall	2396222	0.57
CN1a	Lens drive and feedback connector	---- part of lens	--	--	--	0.00
CN2	Membrane switch input header	FFC / FPC Board Connector, ZIF, Horizontal, 1 mm pitch	68610514422	OneCall	2520120	0.762
CN2a	Membrane switch input connector	Membrane switch input cable White ribbon, 6 ", 152 mm, Same Sided Contact	686605152001	OneCall	252-0192	2.43
CN3	PIC programming header	5 way header	53047-0510	OneCall	9732861	0.37
TS1	Tilt switch	Beam Angle:15°	CW1300-1	OneCall	540614	1.08
-	Printed circuit board (switches) 2-sided	Filename: CSI USB3 camera board 1650.pcb	Part of lens control board	Beta Layout	---	0
SW1-4	Control switches	Focus up, down, sensitivity up-down	SKRBAKE010	OneCall	2056853	0.207
					TOTAL	**29.28**

For completeness, the optical components are listed below in Table 2. All optics are inevitably expensive in small quantities!

Table 2: Optical components

ID	Type	Focal length	Glass	Supplier	Part#	Price
Lens 1	Achromat	45 mm	N-BK7 / N-SF5	Edmund	49-327	58.23
Lens 2	Programmable singlet	120-50 mm (used at 170 to 85 mm)	Polymer	Optotune	EL-10-30-TC	422
Lens 3	Achromat	45 mm	N-BK7 / N-SF5	Edmund	49-327	58.23
Lens 4	Negative singlet	-100 mm	BK7	Comar	100 NB16	27.80
Lens 5	Negative singlet	-100 mm	BK7	Comar	100 NB16	27.80
					Total	**594.06**

6. Performance

The performance of the board was assessed using (1) a high level software interface and (2) oscilloscope measurements of lens current optical focus. Although the lens controller is intended to be ultimately controlled by a host within a complete imaging instrument, it is nevertheless convenient to be able to check the correct operation of the various commands. A Graphical User Interface, shown in Figure 17, was developed in LabWindows (http://www.ni.com/lwcvi/). In addition to displaying the lens temperature and the lens current, the lens optical power (in dioptres) can be set.

Other controls and indicators are self-explanatory and allow us to examine more detailed communication strings, primarily for debugging purposes. Further details of the software and intermediate USB-I^{2}C conversion can be supplied on request. Of course this code is intimately tied to the microcontroller code stored in the PIC.

Checking the dynamic performance of the lens is a little trickier. A high frame rate camera, with a frame period much shorter than the expected response time would have been good to have, but was not available to us. Instead we used the programmable lens to focus light onto a small pinhole of 75 µm diameter. A much larger diameter photodiode detector was placed behind the pinhole and both pinhole and detector

could be translated laterally (i.e. up/down) and along the optical axis. The programmable lens was illuminated with an expanded, collimated, 532 nm laser beam. This arrangement is shown in Figure 18.

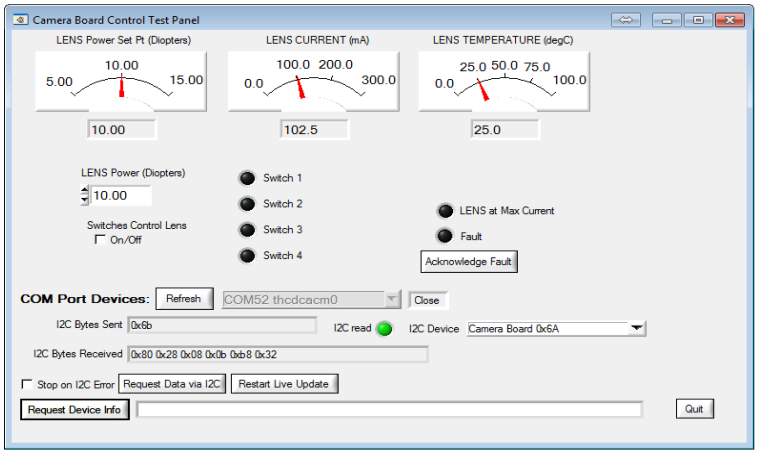

Figure 17. The graphical user interface used to check the operation of the programmable lens and driver.

The photodiode output was connected to the one of the vertical inputs of an oscilloscope, its timebase triggered by the camera sync trigger. The lens dioptre and the XYZ position of the photodiode and pinhole were adjusted to provide a maximum photodiode current. The lens dioptre set-point was then changed (to a higher or lower value) such that the photodiode output was significantly reduced, but not reduced to zero. Once the lens was triggered to move the previous, maximum output dioptre, the settling time following this step change could be determined. For completeness, the lens current waveform was also monitored on a second oscilloscope vertical input channel. Typical results are shown in Figure 19.

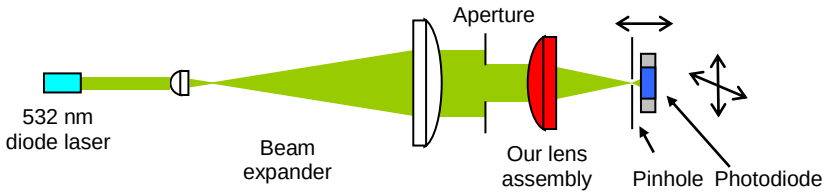

Figure 18. Outline of the optical test rig used to test the dynamic performance of the 28 mm fl lens.

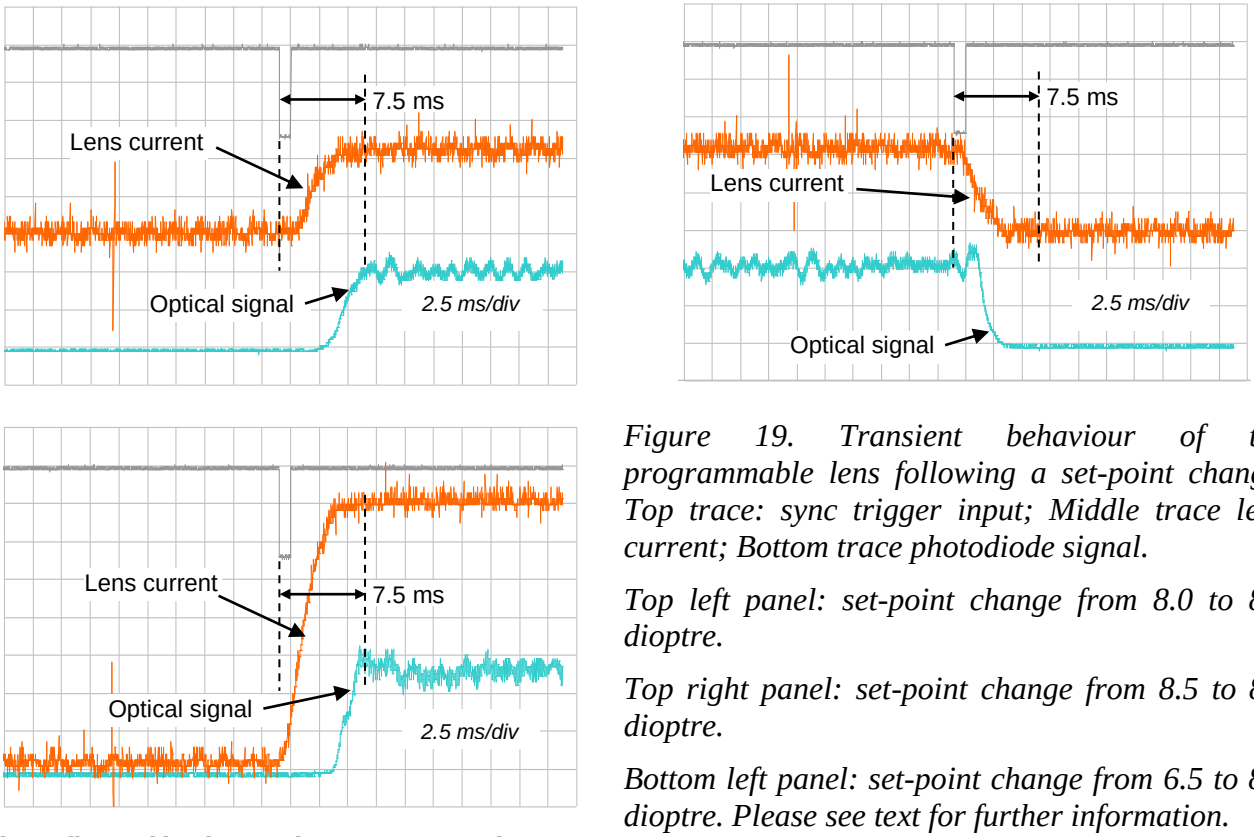

Figure 19. Transient behaviour of the programmable lens following a set-point change. Top trace: sync trigger input; Middle trace lens current; Bottom trace photodiode signal.

Top left panel: set-point change from 8.0 to 8.5 dioptre.

Top right panel: set-point change from 8.5 to 8.0 dioptre.

Bottom left panel: set-point change from 6.5 to 8.0 dioptre. Please see text for further information.

The lens is clearly fast, settling to its new dioptre within a few milliseconds, typically ~7.5 ms at most. By removing the feedback loop, the lens can be of course made somewhat faster, down to 4 ms or so. In practice the additional time makes very little difference since, in our application, the change in focus is triggered by a camera sync signal and this takes place at a rate of 20 or 40 ms. In the top right trace of Figure 19, the response time appears faster, but this is an artefact of our measurement technique: when the focused beam is defocused at the aperture, it does so very fast and the optical trace does not represent the settling time. The 'ripple' in the photodiode signal is caused by laser mode changes and does not represent lens behaviour: we used a very cheap laser pointer type of laser as this was readily available to us. Similar data can be obtained for larger dioptre excursions. Noise in the current trace resulted from unscreened connections; again this does not represent the 'true' lens current. A vertical offset was applied to the lens current trace for clarity. A communication burst some 15 ms prior to camera trigger is also picked up. It was hard to make decent screened test connections on a small board!

Prior to this dynamic testing, the lens feedback loop proportional gain was empirically determined to provide a good current settling time performance. Optotune specify the rise/fall times of the lens to be 3 ms when operating in open loop mode, i.e. when responding to a small signal current step. We could have operated the lens in such an open loop, faster, mode but we could not guarantee that our 12 V-5 V switcher (U4 in Figure 13) would provide a true 5 V output under transient conditions so instead we opted for closed loop control of the lens current. The switching regulator may indeed perform well under transient load changes, but since we wanted to monitor and log the lens current, it was simpler to implement closed loop control rather than extensively check the behaviour of the switcher. In any case, we felt that reliability may be enhanced by not driving the lens with fast current changes. Inevitably, the response time is slightly degraded by implementing closed loop control.

Of course it could be argued that the use of a relatively large 75 μm diameter aperture does not truly represent settling to a true focus: a 5 μm aperture would have been better. We were limited both by the available laser power and by the sensitivity of our detector. In hindsight, we could have expanded the beam less and used a better test setup but there was no reason to expect that the lens speed was worse than that specified by the manufacturer. The oscillograms shown in Figure 19 were intended to show the settling time of the current drive as much as lens performance. Since our current step settles in some 5 ms, the lens settling times closely match the convolution of the inherent lens response and our current step.

It is noted that we based our design on a 'beta' version of the EL-10-30-TC lens and more recent versions cover a slightly different dioptre range and store correction data with significantly improved resolution. In fact the lens-internal data storage is arranged to be compatible with all current and potentially future Optotune lenses. The way that the dioptre settings are defined is also somewhat different. Since we are bound by an agreement with Optotune, we are bound not to reveal these. The interested reader can contact Optotune and obtain more detailed information on these new features. It is slightly unfortunate that Optotune do not readily provide examples of the lens memory decoding. Unfortunately this means that some effort is essential to convert the code to read the lens memory and develop an efficient memory read function. Nevertheless, anyone attempting to a project in which these lenses are embedded will undoubtedly have the necessary skills to write a decoding routine. Of course, once the data have been read and converted into floats inside the PIC, the control algorithms will not change. We have not yet extensively tested the temperature stability of the lens, but will do so in the future and, should anything of interest crop up, we will add an addendum to this note.

So there it is: a compact achromatic programmable lens that can either be used with a small camera on its own or coupled to a laparoscope. One small but important point to consider is that the NIR filter must be removed from the camera C-mount thereby extending detection to the NIR; numerous versions of the camera are available from Point Grey, but the resolution obtainable is limited by the pupil diameters in the laparoscope. Although the lens is indeed achromatic, most laparoscopes are not and this degrades the performance. The chromatic performance of any laparoscope is normally hard to determine since no image is formed. In the future, we will use this lens to establish the chromatic performance of several laparoscopes and hopefully design a lens which corrects for this too. Clearly thicker fluorite glasses will be required and it is unlikely that off-the-shelf optics will be available. However, since NIR imaging at

depth is always associated with scattering, it is not yet clear whether this will be necessary. Nevertheless, when the lens described here is coupled to a laparoscope, the overall performance is superior to that possible with commercial coupling lenses designed to work in the visible. It also permits the use of autofocus algorithms currently under development.

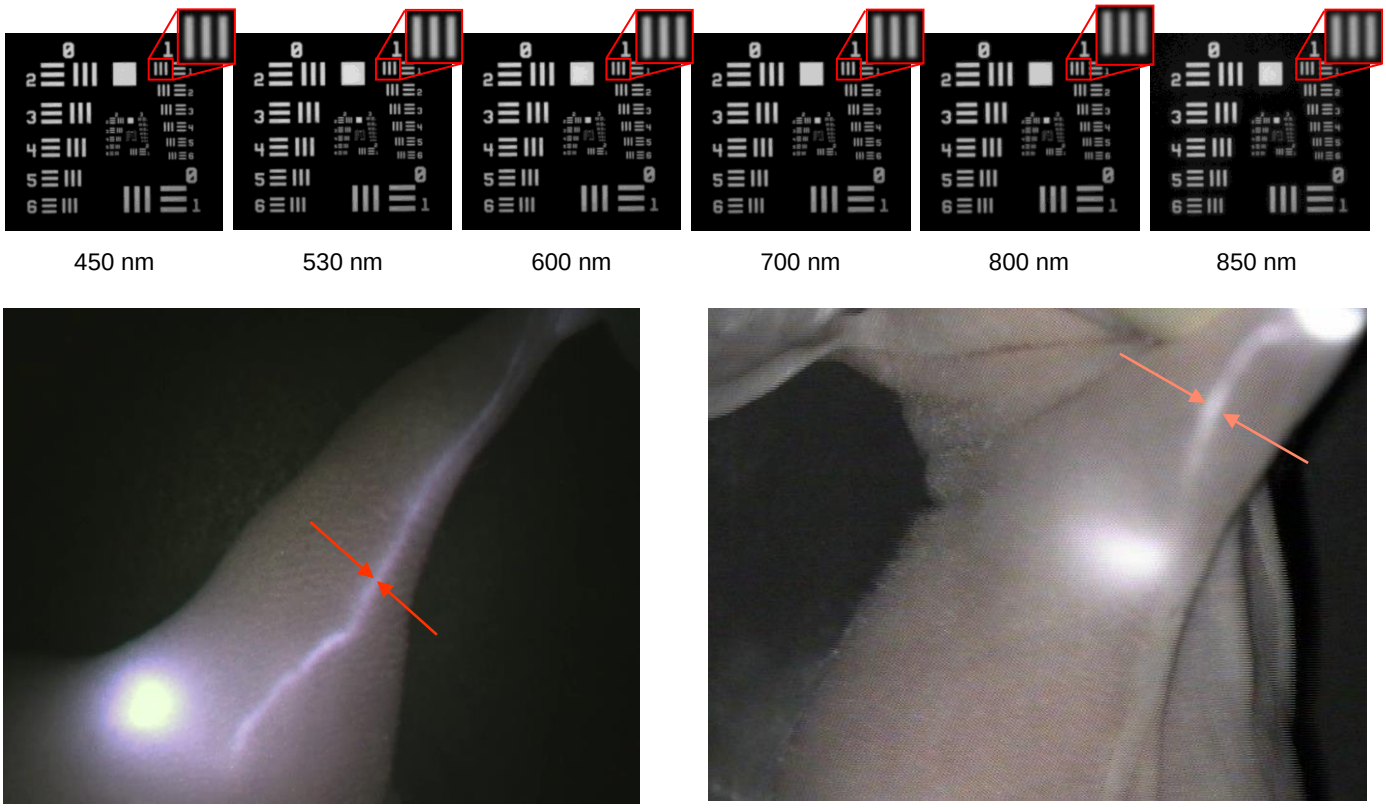

Figure 20. Exemplar images showing the achromatic performance of the lens described in this note. Top images: USAF 1951 resolution chart electronically zoomed images (340 horizontal pixels wide, out of 1280 imaged) acquired over a range of wavelengths. Insets show top right portions of each image magnified ~3.5x and indicate that the perceived resolution is actually pixel-limited by our 1280 horizontal pixel imager. This block of images will be entered in the 'most boring image' competition! Bottom left: NIR-optimised laparoscope coupled to our achromatic lens, image acquired at 40 ms exposure. Bottom right: Free-space optics, image acquired with commercial VIS-NIR corrected lens @ f/5.6 and at 80 ms exposure. Both lower images show the transport of indocyanine green dye through the lymphatic system to a lymph node. Images were acquired using an excitation power density of ~5 mW/cm^2. These indicate the extent of chromaticity introduced by the laparoscope, but also show the improved imaging performance that can be achieved with our lens.

This note was prepared by B. Vojnovic in March 2017. D. Volpi performed all of the optical design and was assisted by I.D.C. Tullis with the mechanics. R.G. Newman designed the printed circuit board and performed electronic construction. Thanks are due to J. Prentice and to G. Shortland for machining the various items. P.R. Barber and I.D.C. Tullis developed the PIC and host interface software.

We acknowledge the financial support of Cancer Research UK